Network Behavior Analysis of Spike Timing Dependent Plasticity (STDP) in Simulated Neural Networks

Vanessa Arndorfer

A Masters Thesis

submitted in partial fulfillment of the

requirements for the degree of

Master of Science in Computer Science and Software Engineering

University of Washington

2025

Committee:

Michael Stiber, Chair

Johnny Lin

Erika Parsons

Dong Si

Program Authorized to Offer Degree:

Computer Science and Systems

University of Washington

Abstract

Network Behavior Analysis of Spike Timing Dependent Plasticity (STDP) in Simulated Neural Networks

Vanessa Arndorfer

Chair of the Supervisory Committee:
Michael Stiber
Computing and Software Systems

The machine learning landscape is rapidly evolving with researchers often turning toward nature for inspiration. Understanding the development of neural networks *in vivo* contributes significant transferable insight for advancing both neuroscience and computational research. This project applies a multiplicative Spike Timing Dependent Plasticity (STDP) model to the weighted graph output from neural growth simulations and analyzes the resulting spike and weight changes over time. This preliminary investigation establishes a baseline process for understanding the effects of STDP on a neural network and provides a framework for defining the resulting network behavior. Through rigorous data analysis, we examine bursting behavior during the refinement phase, analyze the progressive effects of STDP on synapse weights, and compare how the network behavior changes between the growth and refinement phases of neural development.

TABLE OF CONTENTS

LIST OF FIGURES

LIST OF TABLES

ACKNOWLEDGMENTS

I would like to express my most sincere gratitude to my advisor, Dr. Michael Stiber, for his patience, encouragement, and constant support while conducting this research. His guidance and wealth of knowledge is a tremendous inspiration for my continued academic career. I would also like to extend my thanks to my committee members, Dr. Johnny Lin, Dr. Erika Parsons, and Dr. Dong Si, for dedicating their time in support of my thesis.

I am incredibly grateful for the work of the Intelligent Networks Lab members and their tireless contributions to Graphitti. I would like to specifically thank Jasleen Kaur Saini, Haripriya Dhanasekaran, and Marina Rosenwald for their contributions to the STDP simulation code.

Lastly, I could never have accomplished any of this without the incredible support of my friends and family. Thank you to Julie, Allison, and Madison for being my constant cheerleaders; Mariah and Nick for being my guiding pillars; Mom and Dad for believing in me; and my dog, Meeko, for sitting beside me throughout the many late nights.

DEDICATION

To my family,
Mom, Dad, Mariah, Hunter, and Meeko
for always supporting me
no matter how crazy the dream

Chapter 1

INTRODUCTION

Neuroscience research endeavors to expand our understanding of neurons, their connections, and the resulting networks that power the nervous system. Since 1910, scientists have isolated neurons in cortical cultures and electrically stimulated them to simulate neural development, the process by which individual neurons grow into a connected network [23]. Multiple experiments have observed this behavior *in vivo* contributing to our fundamental understanding of how the brain is formed. Computational Neuroscience elevates traditional neuroscience research by leveraging high performance computing for faster simulations and comprehensive data collection.

The Graphitti simulation software, developed by the Intelligent Networks Lab at the University of Washington Bothell, models the neural development process. The program emulates three key stages: nerve cell generation, connection formation, and the strengthening and weakening of synaptic connections. Spike Timing Dependent Plasticity (STDP) emerged as a means to describe changes in synaptic strength during the third phase, the refinement phase, of neural network development [21]. It states that "a presynaptic spike preceding a postsynaptic spike within a narrow time window leads to long-term potentiation (LTP); if the order is reversed, long-term depression (LTD) results" [30]. STDP was implemented in Graphitti in 2021 to modify the magnitude of synaptic strength in line with what is observed in experiments like those by Bell et al. and Bi and Poo [4, 5].

Analyzing the effects of STDP can have significant implications for our medical understanding of the nervous system. Previous research identified Seizure Onset Zones (SOZs) for the treatment of epilepsy using a simulated rat neocortex with STDP [35]. STDP can also lead to synaptic pruning, a process by which synaptic connections are removed from the

network. In 2017, researchers found that neurodegenerative diseases like Alzheimer's and Parkinson's may be linked to a reactivation of developmental synaptic pruning processes like STDP [26]. Building a fundamental understanding of these pruning processes could aid in medical diagnosis of neurodegenerative diseases by identifying regions that are more susceptible to pruning.

Previous research has shown potential applications for modeling neural mechanisms from living organisms in artificial machine learning in a field known as Neuromorphic Computing [29]. The most prominent model in this domain is Spiking Neural Networks (SNNs), which mathematically model neuron spiking behavior for supervised learning [38]. This thesis aims to examine the synaptic strengthening, or potentiation, effect of STDP for potential applications in building artificial neural network architecture. The strengthening of synaptic connections is theorized to be crucial for improving learning and memory and may have transferable effects in machine learning models [2].

The goal of this thesis is to understand the effects of STDP through examining network behavior during the refinement phase of neural network development. Previous works analyzed network behavior during the growth phase by graphing neuron firing rate, burst frequency, and burst shape [18]. In this paper, we apply STDP after the growth simulation, generate comparable metrics between both neural development phases, and discuss how STDP impacts the resulting network.

The analyses explored in this thesis offer the following major contributions: (1) examination of spiking behavior after STDP is applied and a proposed modified definition for bursts in the refinement phase, (2) holistic understanding of synaptic weight progression as a result of STDP, (3) a novel method for distinguishing synapses that strengthen versus weaken over time, and (4) comparative analysis of the growth and refinement phases of neural development.

Chapter 2

BACKGROUND: NEUROSCIENCE BASICS

The below sections provide a brief introduction into fundamental neuroscience concepts needed to understand this thesis.

2.1 Neural Development

The nervous system is an intricate network of cells that transmit signals for controlling behavior throughout the body. It is comprised of two major systems: the central nervous system (CNS), containing the brain and spinal cord, and the peripheral nervous system (PNS) which encapsulates everything else. This system is responsible for processing input, communicating activity, and regulating the body.

Nerve cells, or *neurons*, are the primary cell type which sends signals throughout the nervous system. Figure 2.1 shows the four regions that compose a typical neuron: the cell body, dendrites, axon, and presynaptic terminals [17]. The cell body, or *soma*, contains the nucleus and its time and location of birth determines the neuron's characteristics and function. For example, neurons that develop near a muscle are likely to become motor neurons used for controlling muscle movement. From the cell body, an axon will extend, ending in a presynaptic terminal, for carrying signals to other neurons. Dendrites, on the other hand, branch out in a tree-like fashion and are used to receive electrical signals.

Neurons develop in three key stages, as shown in Figure 2.2. First, nerve cells are generated, unconnected from one another. Next, connections extend from the cells in the form of axons and dendrites, setting up the initial network structure. Lastly, synaptic connections are refined based on the electrical signals they pass [1]. These connections are called *synapses*, where the axon of one neuron, called the *presynaptic neuron*, connects to the den-

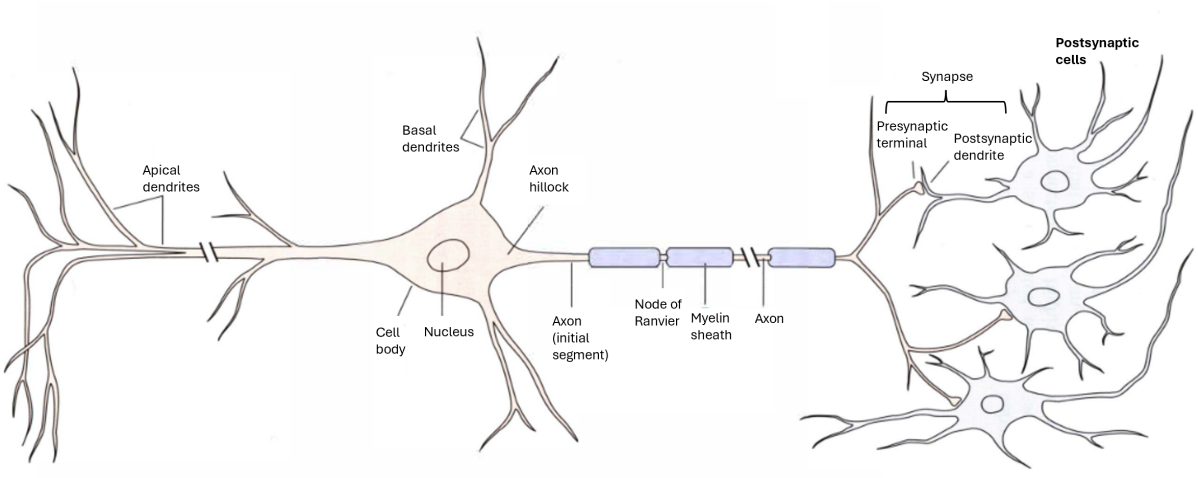

Figure 2.1: Nerve cell diagram by Kandel [17]. Several dendrites extend from the main cell body for receiving electrical impulses from other cells. One axon extends from the cell body as well, terminating in presynaptic terminals for transmitting signals to the awaiting postsynaptic cells.

drite of another, called the *postsynaptic neuron*. For humans, the resulting system contains over 100 billion neurons, each with thousands of connections spanning the network.

2.2 Neural Network Behaviors

When observing neural networks *in vivo*, several interesting behaviors emerge in the interactions between neurons. At the most basic level, one neuron can transmit an electrical signal, also known as a *spike*, to another neuron via synapse. Additionally, elevated synchronous neuronal spiking is a phenomenon known as a *burst*.

2.2.1 Spikes

A neuron spike is when an electrical impulse travels along a synapse. Spiking behavior is determined by the *membrane potential* of the neuron, which is approximately -70 millivolts (mV) at rest. The membrane potential changes, and thus is called a *graded potential*, as

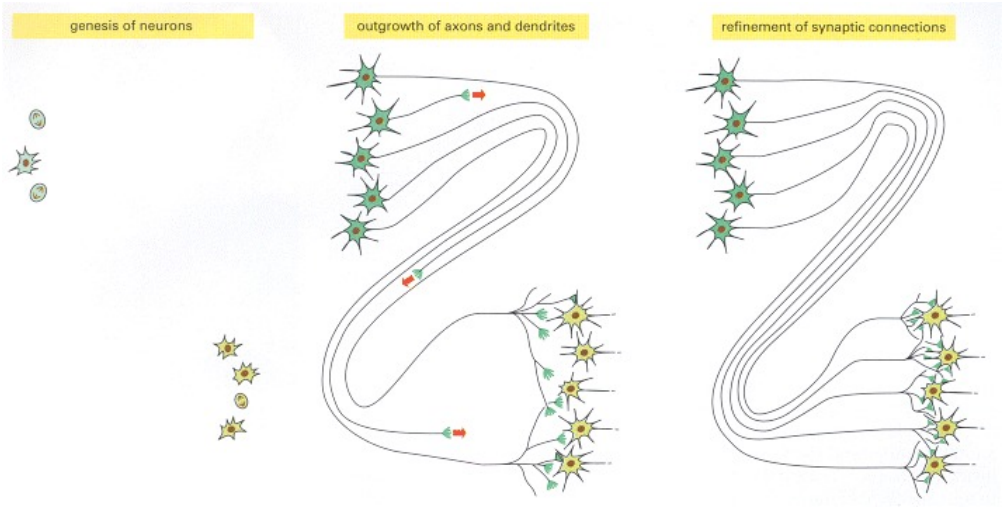

Figure 2.2: Diagram illustrating the three stages of neural development by Alberts [1]. The first stage is composed solely of neurons and an otherwise empty network. Synaptic connections form between neurons in the second phase, known as the growth phase. Finally, the refinement phase is characterized by strengthening, weakening, and pruning of synaptic connections.

charged ions move across the membrane of the neuron cell. A neuron *fires*, or experiences a spike, when the graded potential exceeds the threshold of around -55 mV, turning it into an *action potential*. An action potential is an all-or-none impulse, meaning that all stimuli above the threshold produce a signal of the same amplitude [17]. When a neuron fires repeatedly in a short time period, it is called a *spike train* [24].

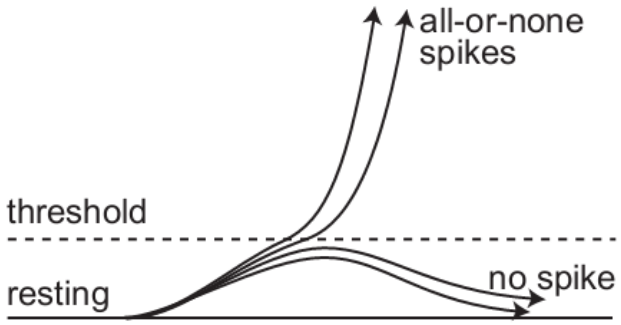

Figure 2.3: Schematic representation of the neuron firing threshold by Gurcan [14]. Electrical potentials begin in a resting state, beneath the threshold, where no spiking behavior can occur. Spikes that exceed the threshold value, approximately -55 mV, become an action potential, characterized as all-or-none and fires to the neuron's max amplitude.

Individual neurons can be classified into two categories, excitatory and inhibitory, that distinguish their contributions to spiking behavior. Each type produces different signals that can change the electric potential and determine when a neuron spikes. Excitatory neurons are neurons that produce glutamate which increases the likelihood of a potential occurring by spurring the movement of positive ions into the cell [27]. The contributions of positive signals have been shown to play a critical role in inducing burst activity [34]. Inhibitory neurons produce y-aminobutyric acid (GABA), a neurotransmitter that decreases electrical activity [9]. Neurons receive streams of both signal types and will only spike when the total of all input signals exceeds the threshold value. After spiking, the neuron experiences a *refractory*

period where it is unable to produce a spike and returns back to its resting potential [28]. Additionally, some neurons are *endogenously active* which means they maintain an oscillation of electrical activity that does not require input from other neurons to spike [3].

2.2.2 Bursts

As a neural network grows and becomes more interconnected, the spikes of one neuron start to trigger spikes in neighboring neurons, heightening the overall activity in the network. A *network burst* occurs when there is elevated bursting activity within a short time window. Often the heightened activity begins at some origin point, propagating through the network and triggering spikes through most or all neurons. Lisman characterized bursts as an important phenomenon for transmitting reliable neural information whereas isolated spikes are more likely to be noise [22].

2.3 Spike Timing Dependent Plasticity

During the refinement phase of neural growth, the connections between neurons can be strengthened, weakened, or pruned entirely. One method for calculating the synaptic strength is Spike Timing Dependent Plasticity (STDP), a form of Hebbian learning which states that neural circuits develop based on correlated activity [33]. In STDP, synapses are refined based on the spike timing between neurons and the spiking pattern within each neuron [12, 21]. If a presynaptic spike occurs shortly before a postsynaptic spike then the synapse weight is strengthened, resulting in long-term potentiation (LTP). Otherwise, if a postsynaptic spike precedes a presynaptic spike within a short time window, then long-term depression (LTD), or a weakening of synaptic strength, results [30].

In their 2002 paper, Froemke and Dan formulated a multiplicative model for STDP, described in Equation 2.1. The model takes the time difference between the ith presynaptic spike and the jth postsynaptic spike to get $\Delta t = t_j^{post} - t_i^{pre}$ as input. The function $F(\Delta t)$ yields the estimated contribution of each pre/post spike pair to the synaptic weight modification, where A is a scaling factor, τ is a time constant, $+$ is LTP, and $-$ is LTD. In

the multiplicative model, the net effect of the spike train is the product of each spike pair: $1 + \Delta w = \prod_{ij}(1 + \Delta w_{ij})$.

$$\Delta w_{ij} = F(\Delta t) = \begin{cases} A_+ e^{-|\Delta t|/\tau_+} & if \quad \Delta t > 0 \\ A_- e^{|\Delta t|/\tau_-} & if \quad \Delta t < 0 \end{cases} \tag{2.1}$$

The resulting graph, shown in Figure 2.4, for the STDP multiplicative model shows the amount of synaptic weight change, Δw_{ij}, as Δt changes. Pre/post spike pairs within a shorter time window will experience a more significant change in synaptic weight. The STDP gap is visible between the two curves when Δt is close to zero.

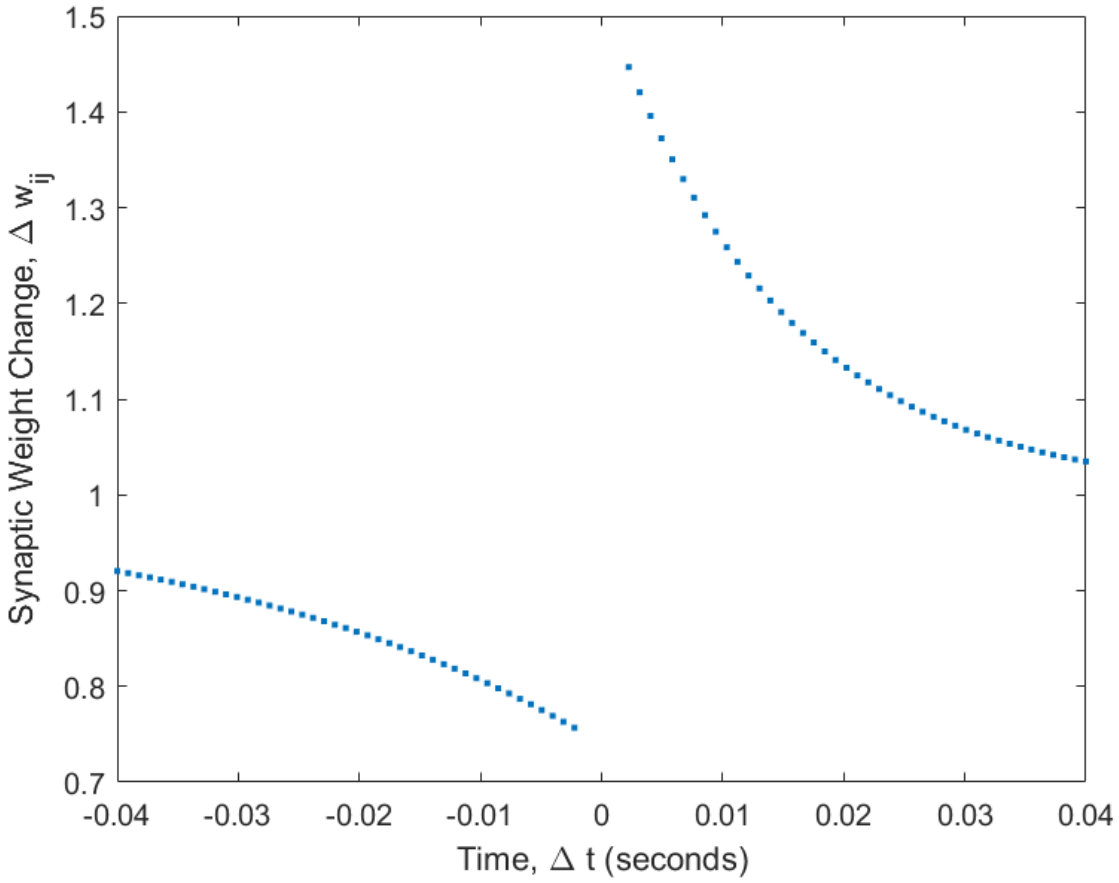

Figure 2.4: Critical window for synaptic modifications generated using the weight modification function from Singh [32]. Spikes within a shorter time window experience a greater magnitude of synaptic change.

Chapter 3
METHOD: DATA ACQUISITION

Traditional analysis of neural development *in vitro* involves isolating cortical cells, applying extracellular stimulation with multi-electrode arrays, and observing any excitatory postsynaptic potentials [25, 12]. These living neurophysical preparations are time consuming, taking several days before connections form and requiring months of care and observation by scientists [7]. In 2014, Kawasaki and Stiber remedied these limiting factors in the BrainGrid, now Graphitti, simulation framework. Graphitti implements a leaky-integrate-and-fire model which ignores the underlying physiological behavior while still producing neuron spiking behavior for observation [18].

3.1 Graph Initialization

The Graphitti simulation is initialized with a graph layout defined by neurons (nodes) and, optionally, synapses (edges). Neurons are configured in a repeated 10 x 10 pattern to equally distribute the different neuron types and eliminate variability that can be introduced with a randomly generated graph. The neuron pattern that was established by Kawasaki to maximize the distance between endogenously active and inhibitory neurons. The layout is redrawn by Singh in Figure 3.1 [18, 32]. The full network graph contains 10,000 neurons arranged in a 100 x 100 square array, composed of this repeated pattern.

3.2 Growth Simulation

An unconnected graph, input into a growth simulation, simulates how synapses form between neurons over a period of time. A neuron's capacity for connection is tracked using radii of connectivity, where an overlap of radii between two neurons forms a connection. The weight

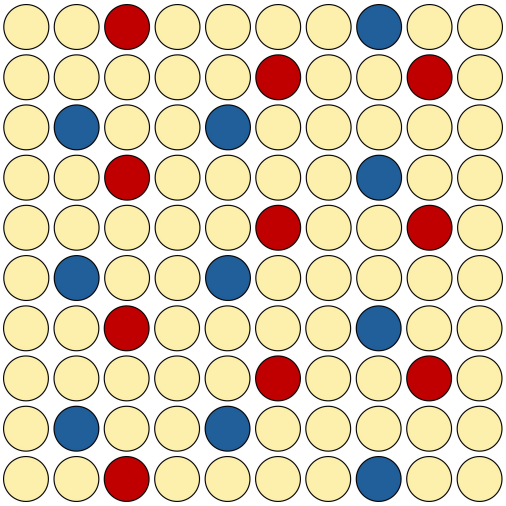

Figure 3.1: Example 10 x 10 neuron layout from Singh [32]. Endogenously active neurons are indicated in blue, inhibitory neurons are red, and excitatory neurons are yellow.

for each connection is calculated by the area of neuron radii overlap, normalized by a factor of 10^7 [32]. Since the area of overlap is shared between the two neurons, the resulting edge weight is equal in both directions, forming an undirected weighted graph.

3.3 STDP Implementation

This work uses a simplified implementation, originally developed in Singh 2021, of Froemke and Dan's STDP multiplicative model [32]. The effects of STDP are encapsulated by two algorithms: Algorithm 1 *stdpLearning()* which applies the cumulative effect of pre/post spike pairs to the edge weight and Algorithm 2 *synapticWeightModification()* which calculates the the fractional change caused by each individual pre/post spike pair.

The code relies on dynamic synapses which are synapses that exhibit a refractory period after spiking. While dynamic synapses are not required to observe the effects of STDP, the refractory period affects how frequently a neuron can spike and is consistent with the synapse model used during the growth simulation. The STDP model, as detailed in Section 2.3, can be configured before simulation execution with the values for A and τ to adjust how rapidly

Algorithm 1 stdpLearning()

Require: $|time\_interval| > STDP\_Gap$

$delta\_w = 1 + synapticWeightModification()$

if $delta\_w \neq 0$ **then**

$weight \leftarrow weight \times delta\_w$ ▷ Multiplicative Model

end if

if $|weight| > max\_weight$ **then**

$weight \leftarrow max\_weight$

end if

Algorithm 2 synapticWeightModification()

if $time\_interval < -STDP\_Gap$ **then** ▷ Depression

$delta\_w \leftarrow$ Aneg $\times$ exp(time_interval / tauneg);

end if

if $time\_interval > STDP\_Gap$ **then** ▷ Potentiation

$delta\_w \leftarrow$ Apos $\times$ exp(-time_interval / taupos);

end if

return $delta\_w$

synaptic weight changes.

3.4 Simulation Workflow

In Graphitti, the development of the nervous system can be replicated in two simulation executions. First, a growth simulation is run on an initially unconnected neuron array, defined within a graphml file. As the simulation progresses, synapses form between neurons, a process that takes nearly 28 days *in vivo* [31].

At the end of a simulation, three key data structures are collected for analysis:

- **HDF5 Recorder Output** - An HDF5 file containing the spike history for every neuron. Each neuron that exhibited spiking behavior has a corresponding HDF5 dataset, named in the format "Neuron_#." Each element in the neuron dataset is a timestep when the neuron spiked.

- **Weights Matrix** - A $totalNeurons \times maxEdgesPerVertex$ matrix containing the weight of each synapse at the end of the simulation. The row index corresponds to the destination neuron. The matrix is zero-padded for neurons that have fewer connections than the max allowed value.

- **Source Neuron Matrix** - A $totalNeurons \times maxEdgesPerVertex$ matrix containing the source neuron for each non-zero value defined in the Weights Matrix. Similar to the weight matrix, the row index corresponds to the destination neuron and the matrix is zero-padded for neurons that have fewer connections than the max allowed value.

At the end of the growth simulation, the matrices defined above are parsed to generate edge definitions which are appended to the original graphml file for input into the STDP simulation. This method retains synapse configuration across simulation instances, defining each synapse by the presynaptic neuron id, postsynaptic neuron id, and edge weight.

3.4.1 Simulation Configuration

Each simulation array is defined by the *fraction of excitatory neurons*, f, which is equal to the percent of excitatory neurons that make up the network. In the growth simulation, a *target rate* (ϵ) can also be varied to control the max neuron firing rate. Bursting behavior was observed in growth simulations when ϵ is 1.0Hz or 1.9Hz with 90% or 98% excitatory cells [18]. We chose $\epsilon = 1.0$ and $f = 0.90$ for the initial data analysis to establish baseline processes for handling spike and weight data. The growth output was then input to the STDP simulation for comparison. Parameters for the Growth and STDP simulations are given in Table 3.1.

Table 3.1: Growth and STDP Configuration for the Graphitti Simulation

Simulation Type	Epochs	Epoch Duration (sec)	Total Duration (sec)
Growth	600	100	600,000
STDP	25	1	25
STDP	100	1	100
STDP[1]	100	10	1000

For STDP, most parameters were configured according to the values described in [12]. However, the scaling factor, A, was halved ($0.5A$), slowing the effect of STDP and facilitating observation of the STDP weight modification over time. These values are detailed in Table 3.2. For simplicity, the τ and A values are identical for both excitatory or inhibitory neuron types. Finally, the max synaptic weight was configured to a limit of 5.0265×10^{-7} based on previous simulations.

[1]Due to time and memory constraints the weight matrix in the longest simulation was collected every 10 seconds instead of every 1 second. Further analysis will focus on the 25 and 100 second STDP simulation results, while the 1000 second simulation is only used to estimate long term trends.

Table 3.2: Scaling factor, A, and time constant, τ configuration for the STDP simulation

Parameter	Positive (+)	Negative (-)
τ	0.0148	0.0338
A	0.52	-0.26

These simulations were executed on an Intel(R) Xeon(R) Gold 5118 CPU @ 2.30GHz processor with a Debian GNU/Linux 10 OS. The growth simulation was run on an NVIDIA Tesla V100 GPU with CUDA 11.2 libraries.

Chapter 4
METHOD: DATA ANALYSIS

The novel Graphitti implementation detailed in Chapter 3 allows for simultaneous collection of neural spiking behavior and synaptic weight evolution data. The study of neural spiking behavior has a rich history that has uncovered phenomena like bursting and avalanche patterns during neural growth. Synaptic weight evolution is less frequently studied, with most research analyzing weights in terms of network structure. This presents a unique opportunity to understand synaptic weight behavior over time and establish a standard for preparing weight data for analysis. In this section, we lay the foundation for analyzing spiking behavior during the refinement phase by extending the analysis methods developed in the growth phase. Additionally, we develop processes for examining synaptic weight over time and propose methods for correlating spiking behavior, weight behavior, and neuron types.

4.1 Spiking Behavior

Neuron spikes are the most basic indicator of information processing in the nervous system. The transfer of these electric potentials along synapses is key to identifying how information flows through a neural network [11]. Spiking behavior provides insights on the per-neuron level and can be generalized to the entire network, revealing larger trends for describing network behavior and identifying interesting phenomena.

4.1.1 Average Per Neuron Firing Rate

Average Per Neuron Firing Rate (APNFR) is a metric used to analyze whole network spiking behavior using individual neuron spike times [10]. APNFR is calculated as the number of spikes per second (Hz), normalized by the number of neurons. Analyzing APNFR changes

over time can help identify periods of elevated firing rate indicative of bursting behavior and is used to identify the burst threshold described in Section 4.2.1.

4.2 Burst Identification and Behavior

4.2.1 Burst Threshold

Previous research identified bursts using a binning method to summarize the number of spikes every 10 milliseconds. Bins that exceeded a burst threshold of 0.5 Hz/neuron or 50 spikes/bin were classified as belonging to a burst, with the burst terminating when APNFR returned below the threshold. After identifying all bursts, additional information is collected to distinguish intra-burst and inter-burst behavior.

4.2.2 Burst Percentage

Burst percentage was calculated by totaling the number of bins above the burst threshold and dividing by the total bins in a given simulation. The result estimates the amount of time the network exhibits burst behavior. This metric offers a singular data point to describe the percentage of time a network experiences elevated spiking behavior correlated with bursting versus periods of rest.

4.2.3 Burst Visualization

Spatiotemporal analysis was extended to the spike train data by generating movie visualizations that reveal how bursts propagate through a network. This process, established in Lee 2018, represents the network as 100x100 grid, where each pixel correlates to a neuron at their corresponding (x, y) location [20]. The color of each pixel (neuron) is determined by the number of spikes fired by the neuron in a 10ms time bin. These images were either output individually or concatenated to generate a burst movie.

Figure 4.1: Example spike training binning of a 5 x 5 neuron array from Lee [20]. Each pixel displays the number of times the neuron spiked for a single bin. The color of each square is determined by the spike count at that (x, y) location, where brighter colors indicate higher spike rate.

4.3 Long Term Weight Evolution

STDP stipulates that synaptic weights that grow in magnitude over time experience Long-Term Potentiation (LTP), whereas synapses whose weights approach zero, experience Long-Term Depression (LTD). Weights that narrowly approach zero may indicate that the synapse is pruned from the network. Similarly, weights that experience significant strengthening over time are hypothesized to be part of important neural pathways for disseminating information.

During STDP, the simulation outputs a weight matrix every second which was then parsed into a $numberOfSynapses \times simulationLengthInSeconds$ weight evolution matrix to show the per synapse weight change over time. The long term effects of STDP can be approximated by taking a synapse weight at the end of the simulation and subtracting it from the synapse weight at the beginning of the refinement phase.

4.3.1 Synaptic Weight Types

At the end of the growth simulation, the resulting weight matrix is symmetric where the magnitude of an edge from $A \rightarrow B$ is equal to the magnitude of the edge from $B \rightarrow A$. The sign of an edge weight is determined by the presynaptic (source) neuron, where the synaptic

weight is positive for excitatory synapses with excitatory presynaptic neurons and negative for inhibitory synapses with inhibitory presynaptic neurons. Separating analysis by synaptic weight type can expose trends in how the effects of STDP differ between inhibitory and excitatory edges.

4.4 Spearman Correlation

Spearman correlation generates a similarity score between two variables and can determine if the variables have a monotonic relationship. This definition is more flexible than the Pearson correlation for linear relationships which requires an assumption that the data is normally distributed. Spearman correlation is denoted by $-1 < \rho < 1$ where the lower bound indicates a decreasing monotonic trend and the upper bound an increasing monotonic trend. For each ρ, a p-value is calculated to test the statistical significance of the results. P-value provides the probability that the correlation results are caused by chance, where a small p-value indicates higher confidence in the correlation.

The statistical similarity between two ranked variables is calculated using Equation 4.1, where d_i is the difference between the ranks of corresponding variables and n is the number of observations. Ranks are created from discrete or continuous data by assigning each element a numerical order from smallest to largest value.

$$\rho = 1 - \frac{6 \sum d_i^2}{n(n^2 - 1)} \tag{4.1}$$

For neural simulations, this formula is used to generate a numeric quantity indicating any monotonic relationship between neuron types and the weight of the synapse between them. This paper hypothesizes that synapses with endogenously active or excitatory source neurons are more likely to experience long-term potentiation. Conversely, synapses with inhibitory source neurons are hypothesized to experience long-term depression.

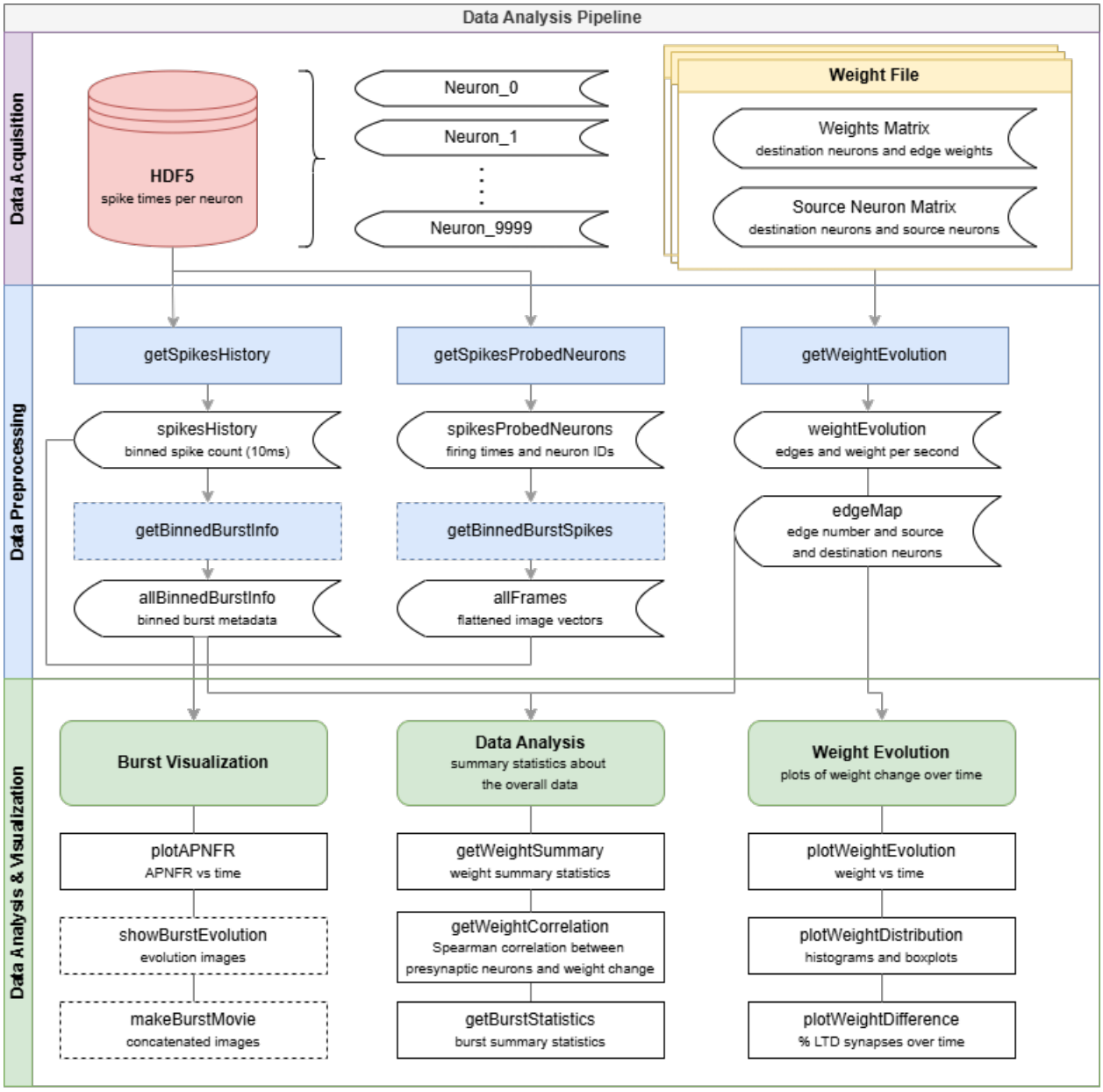

Figure 4.2: Workflow diagram of the data analysis process used to generate, process, analyze, and visualize the STDP spike and weight data. Functions outlined with a dotted line were repurposed from Lee 2018 [20]. Preprocessing functions (highlighted in blue) were written in both Matlab and Python. Data analysis functions (categorized in green) were written entirely in Matlab.

Chapter 5

RESULTS

5.1 Burst Characteristics

5.1.1 Burst Shape

After bursts were identified using the threshold from Kawasaki and Stiber and the code from Lee, APNFR was graphed, revealing the burst shape difference before and after STDP [18, 20]. In Figure 5.1, the first burst is consistent with burst shapes during the growth simulation, rising above the burst threshold for a short time before returning to zero. The effect of STDP changes the burst shape to multiple peaks above the burst threshold over a longer time period.

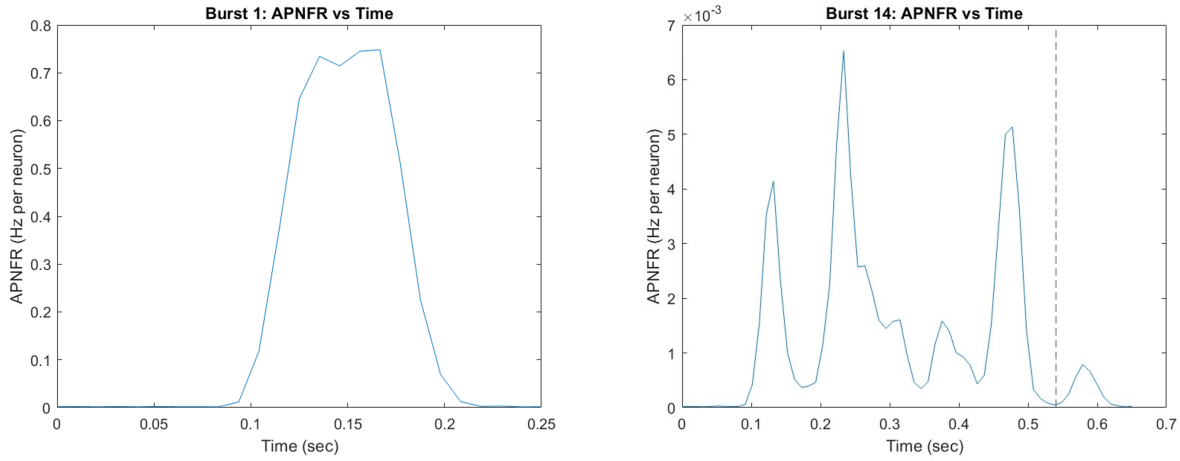

Figure 5.1: Comparison between the 1st (left) and 14th (right) burst in the STDP simulation, using the burst definition from [18]. The first burst is representative of a burst during the growth phase and the fourteenth of a burst after STDP takes effect. The dashed line in the right graph indicates the start of the next burst.

Table 5.1: Summary statistics of the growth simulation and 100 second STDP simulation

Metric	Growth	STDP
Average Width (ms)	163.0	99.6
Average Spikes per Burst	45,469.30	11,010.50
Average Interval (ms)	6032.2	185.8
Burst Percentage	2.70	53.57

During burst identification, we collected additional information including the number of spikes per burst, burst width, and the interval between bursts. The 100 second STDP simulation had 538 total bursts with an average width of 99.6 ms. Comparatively, the average burst in the growth simulation had a width of approximately 163 ms as shown in Table 5.1. Growth bursts also contained four times as much spiking activity as STDP bursts.

Bursts were more common during the STDP simulation as indicated by the average shorter interval between bursts and higher burst percentage. Burst percentage was calculated from spike history by totaling the amount of time spent above the burst threshold and dividing by the total simulation time. Overall, growth bursts are wider with approximately 4 times more spikes than bursts after STDP, however the STDP simulation exhibits bursting behavior 50.87% more frequently.

In Figure 5.2, a spatiotemporal visualization of the network was generated to show how bursts evolve over time. The burst progresses as a series of snapshots where each pixel is a neuron and the brighter color indicates higher spike rate. The first burst is consistent with bursts during the growth phase, beginning at a singular origin point and expanding as a circular wave to the edges of the network. In the next burst, the burst wavefront becomes asymmetric, exhibiting a heart shape as opposed to the circular wavefront. The asymmetric burst shape evolves further by the fourth burst which first moves towards the southern edge of the network before inverting to capture the rest of the network. Lastly,

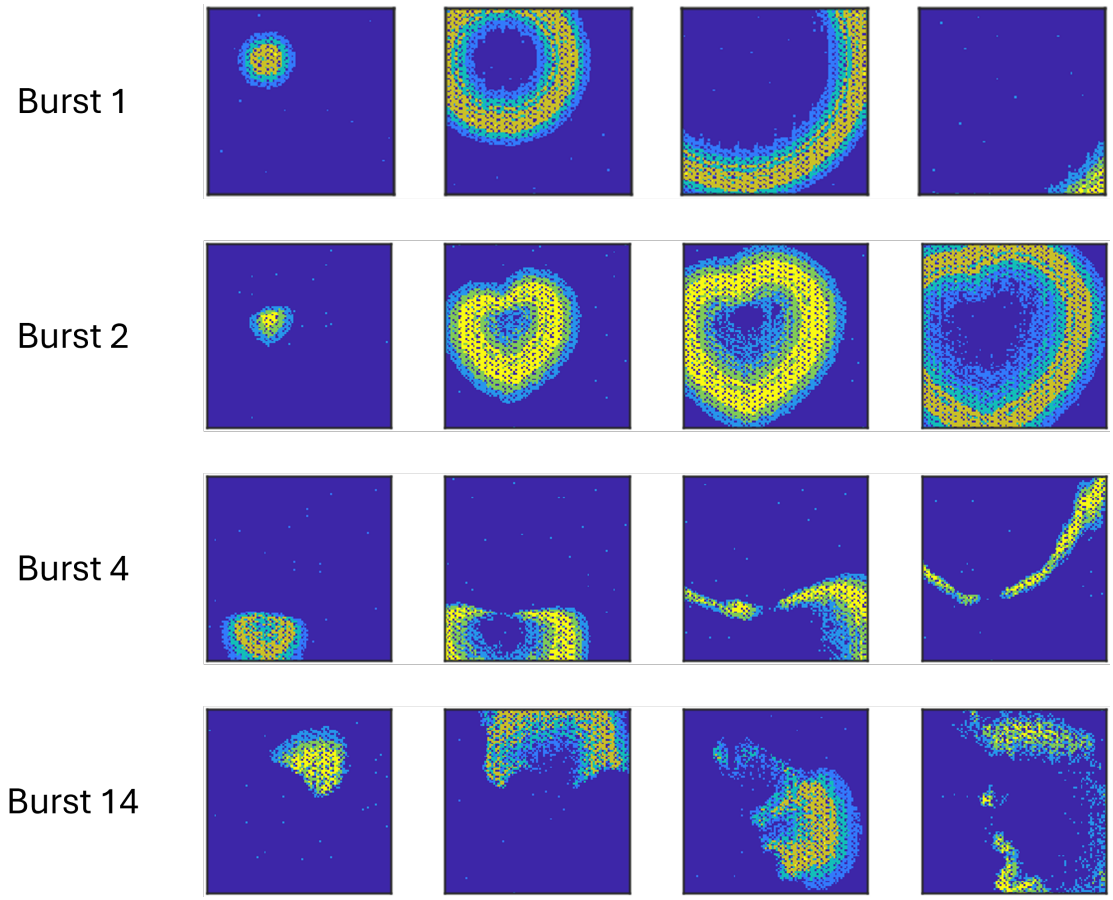

Figure 5.2: Spatiotemporal burst evolution comparison between the first, second, fourth, and fourteenth bursts of the STDP simulation, using the burst definition from [18].

burst behavior becomes less uniform by burst 14, revealing several small clusters of activity as the burst progresses. As a result, bursting behavior is preserved across the growth and STDP simulations, however burst shape changes from uniform waves of activity to multiples wavefronts with high spiking rate in a short period of time.

5.2 STDP Weight Modification Characteristics

5.2.1 Synaptic Weight Summary Statistics

At the end of the growth simulation, the network formed 409,424 weighted edges. Table 5.2 shows that 94.36% were excitatory edges with positive synaptic weight and 5.64% were inhibitory with negative synaptic weight.

Table 5.2: Distribution of excitatory and inhibitory synapse

Synapse Type	Number of Edges	Percentage
Excitatory (+)	386,340	94.36%
Inhibitory (-)	23,084	5.64%

These edges were then input into the STDP simulation and their weights were tracked per second. Figure 5.3 and 5.4 show a histogram distribution of the synaptic weight for the 25 second simulation. The distribution remains the same for the first 12 seconds before the first burst. After the first burst, the distribution spreads along the positive synaptic weight axis for excitatory synapses affected by LTP, and towards zero for synapses affected by LTD. As time progresses, a bimodal distribution develops with most synaptic weights approaching zero and a subset approaching the maximum configured weight limit, 5.0265×10^{-7}. This plot was also generated for the 100 second simulation and the distribution remained consistent with the data at 25 seconds, so no new information was gained from graphing the distribution of the longer simulation.

Figure 5.5 shows the synaptic weight distribution in the form of boxplots at four points of interest in the simulation, where 13 seconds is the distribution after the first burst. This plot allows for clearer visualization over the histogram binning method to show the weight progression towards a synaptic weight value of zero. Table 5.3 provides the quartile data used to generate the distribution boxplots, revealing a clear trend where most synapse weights

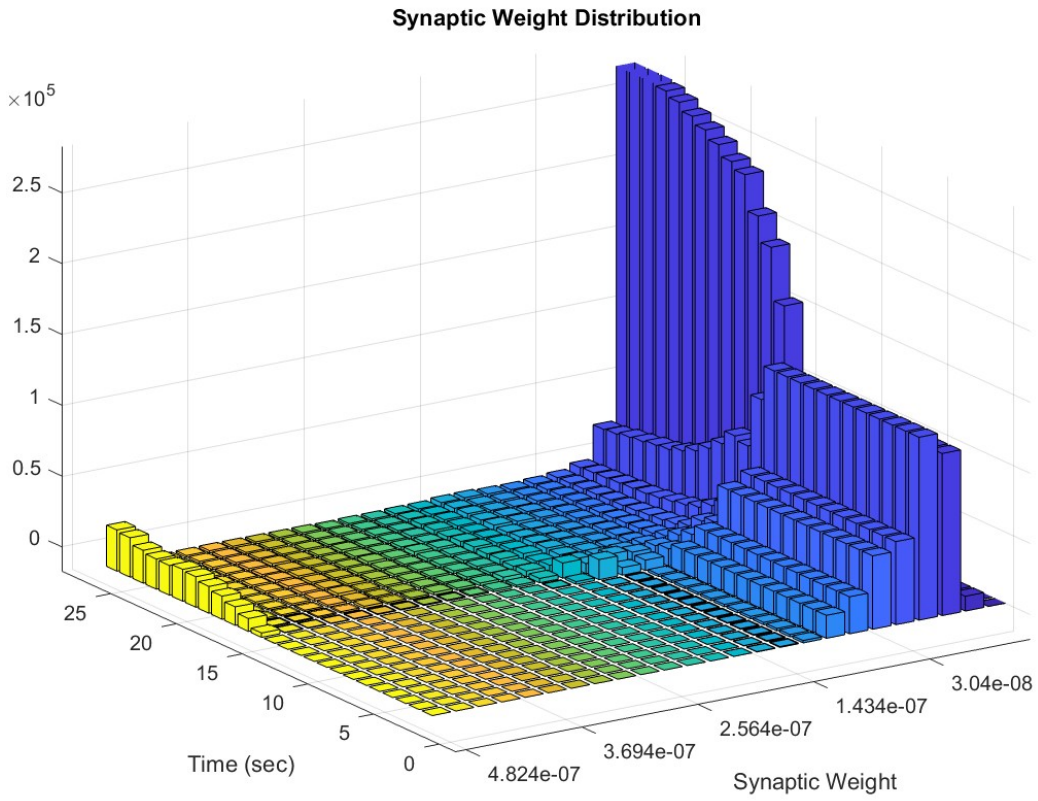

Figure 5.3: Histogram distribution of synaptic weights over time. Most synapses have a near-zero weight a small portion approaching the max synaptic weight value as time progresses.

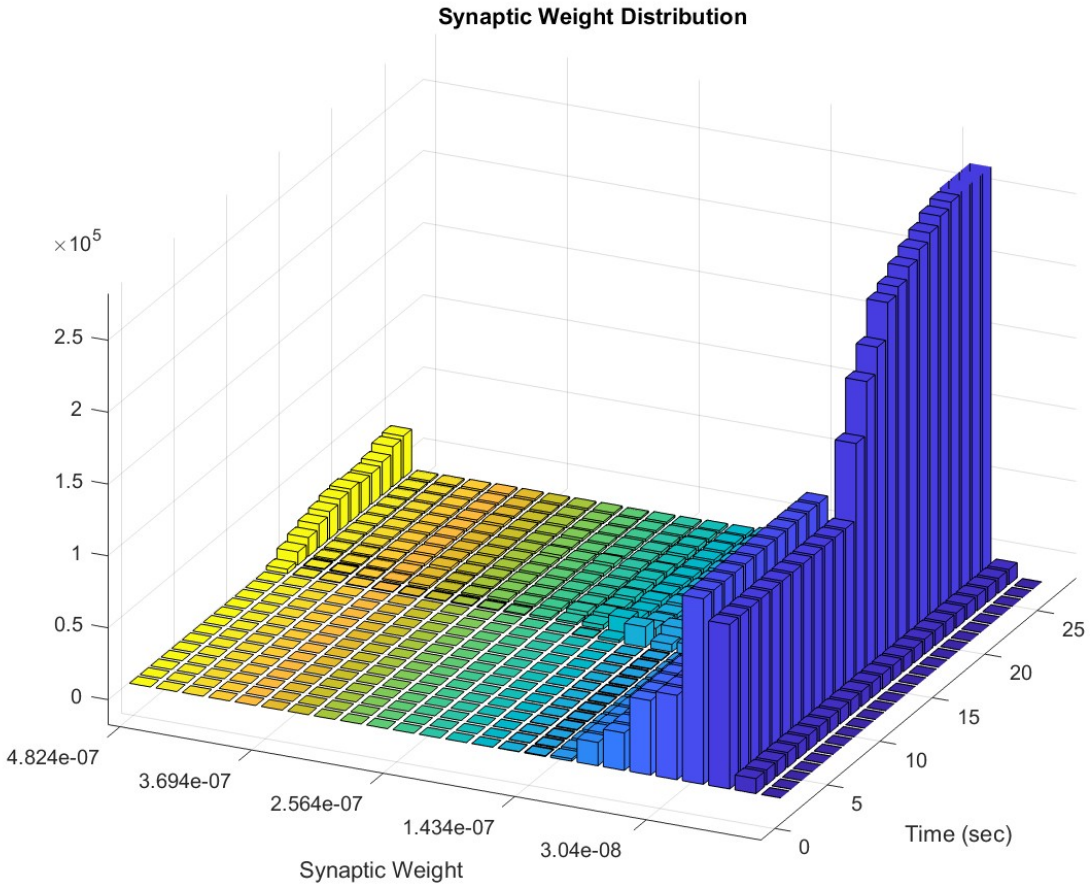

Figure 5.4: Histogram distribution of synaptic weights over time rotated from Figure 5.3, showing the bin containing negative synaptic weights.

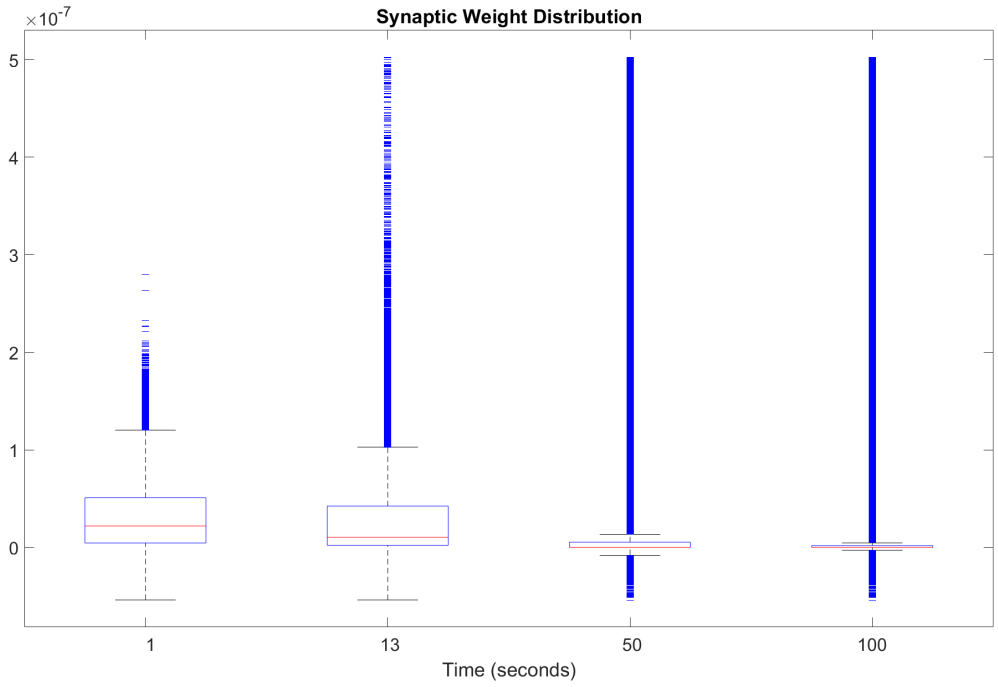

Figure 5.5: Synaptic weight distribution for the STDP simulation. Boxplots were generated at the simulation start (1), after the first burst (13), halfway through the simulation (50), and at the end of the simulation (100). Outliers are indicated by a blue line (-).

Table 5.3: Quartile values used to generate the boxplots in Figure 5.5. The first quartile and median values indicate an exponential increase in synapses that approach zero.

Time (s)	First Quartile	Median	Third Quartile
1	4.60×10^{-9}	2.20×10^{-8}	5.09×10^{-8}
13	2.16×10^{-9}	1.04×10^{-8}	4.24×10^{-8}
50	7.55×10^{-29}	5.90×10^{-15}	5.40×10^{-9}
100	7.29×10^{-44}	1.18×10^{-19}	1.89×10^{-9}

approach zero over time. By the end of the simulation, the first quartile and median values indicate that a quarter of the data has decreased exponentially towards zero between 10^{-19} and 10^{-44}. The third quartile value decreased less significantly from 10^{-8} to 10^{-9}. Additionally, after the first burst, the synaptic weights continue to span the same minimum and maximum range, showing that no weights moved further in the negative direction.

5.2.2 Long Term STDP Effects

From the synaptic weight progression, we approximated which synapses experienced overall Long Term Potentiation (LTP) versus Long Term Depression (LTD) by calculating the difference between the weight at the end and beginning of the simulation. Weights that experienced positive synaptic weight change were categorized as LTP and negative change as LTD. Table 5.4 shows that 71.42% of synapses experienced depression, or a trend toward 0, after 100 seconds. Figure 5.6 tracks the percentage of LTD synaptic weight change each second, concluding that the percentage of depressed synapses is consistently around 70% as the simulation progresses and these synapses will likely see a steady weight progression toward zero.

In Figure 5.7, the synaptic weight progression of a singular LTP synapse is graphed over time. The graph reveals that this method introduces some variability as LTP synapses

Table 5.4: Distribution of synapses that experienced overall LTP, LTD, or no weight change after a 100 second simulation.

Synaptic Change	Number of Edges	Percentage
LTP	70,876	17.31%
LTD	292,408	71.42%
No Change	46,140	11.27%

experience irregular weight changes between near-zero and the maximum configured synaptic weight value. The example synapse is categorized as LTP after 100 seconds, however if the simulation had ended at 80 seconds, then it would have been categorized as LTD. A random sample of 50 LTP synapses is graphed for the 1000 second simulation in Figure 5.8 to see if the weights stabilize over time. From the graph, the weights change more frequently in the first 250 seconds, with some stabilizing to a constant value for the remainder of the simulation.

After grouping synapses by LTP, LTD, and no weight change after 1000 seconds, the data was further separated by excitatory and inhibitory synapses to identify trends in their long term synaptic weight change. 11.27% of synapses did not experience any change in weight between the start and end of the simulation. Table 5.5 reveals that all inhibitory synapses fell into the "no change" category, maintaining a constant synaptic weight that was unaffected by STDP. Excitatory synapses were graphed separately based on whether they potentiated, depressed, or had no change. Despite the variability revealed in Figure 5.7, this estimation is sufficient to identify long term trends as shown in Figure 5.9. The average LTD synaptic weight approached zero and the average LTP weight had a positive increasing trend as hypothesized.

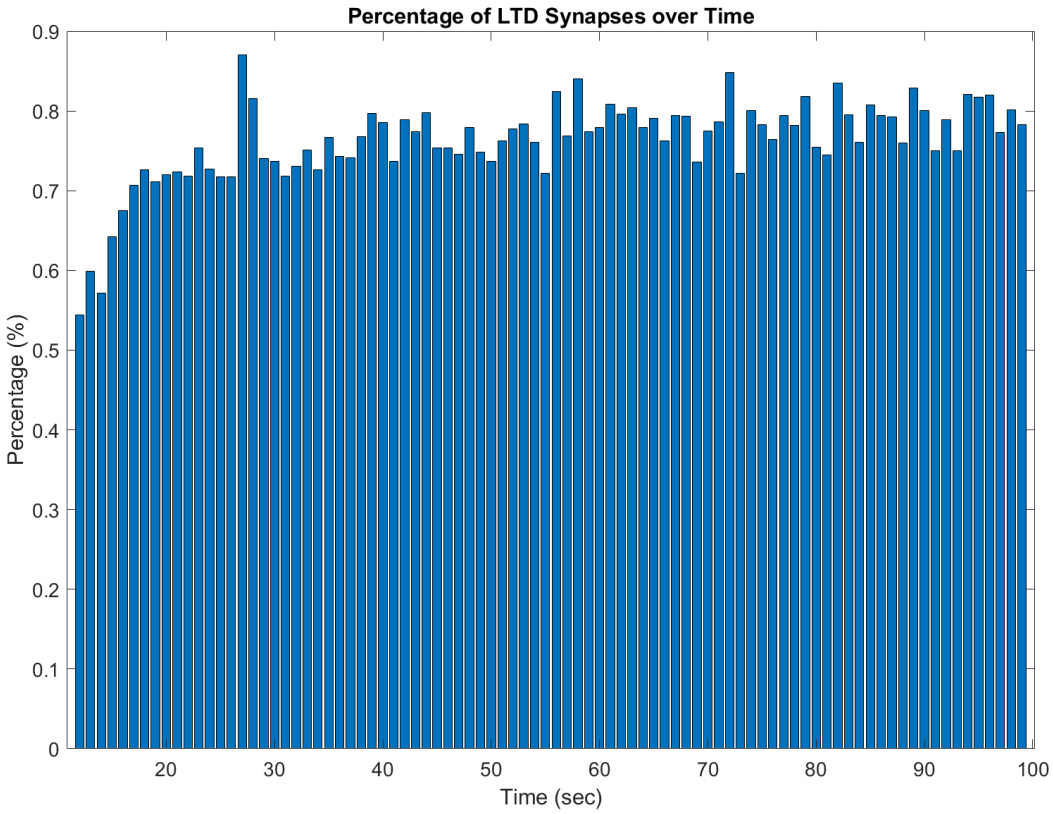

Figure 5.6: The percentage of synaptic weights that decreased each second when compared to the previous one (LTD) for each second of the simulation.

Table 5.5: Distribution of synapses by type that experienced overall LTP, LTD, or no weight change after a 1000 second simulation.

Synapse Type	Weight Change	Number of Edges	Percentage
Excitatory	LTP	38,373	9.37
	LTD	324,885	79.35
	No Change	23,082	5.64
Inhibitory	No Change	23,084	5.64

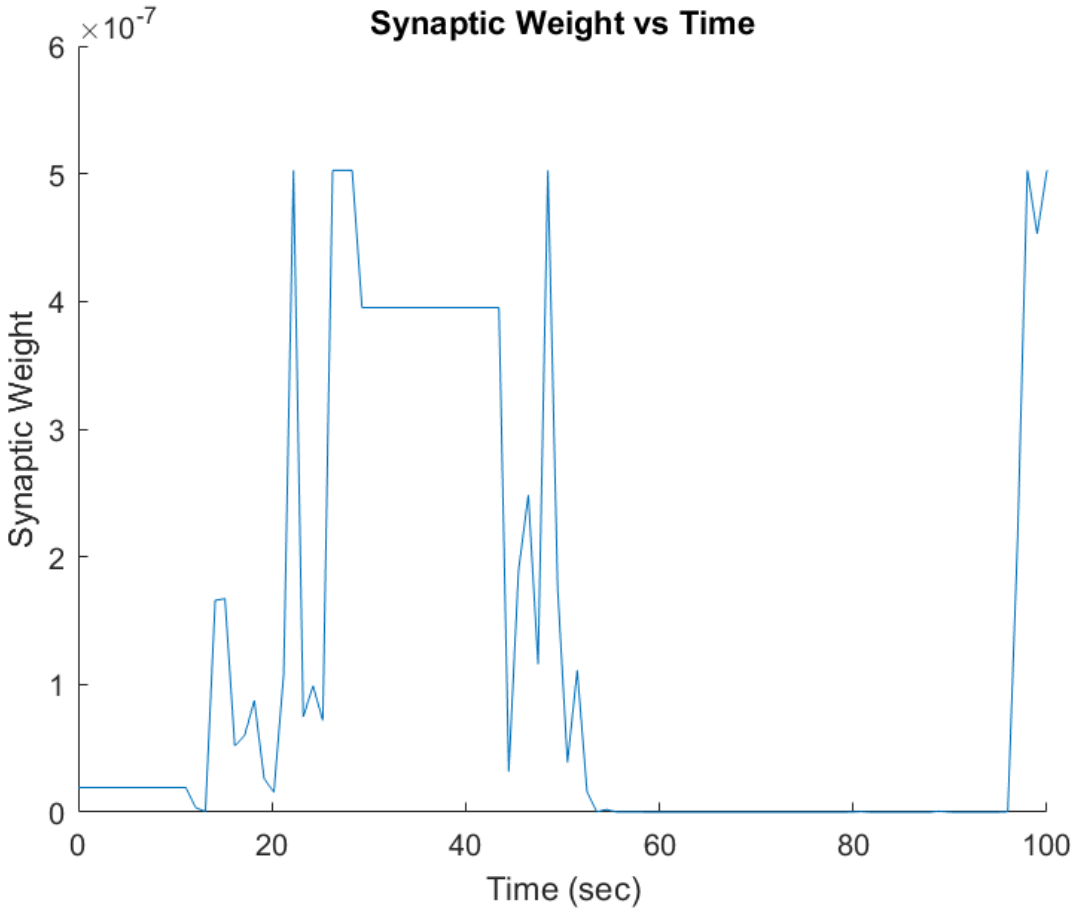

Figure 5.7: Example synaptic weight progression over time of a single LTP synapse. Although the synapse was classified as LTP at 100 seconds, had the simulation ended at 80 seconds, the synapse would be considered LTD.

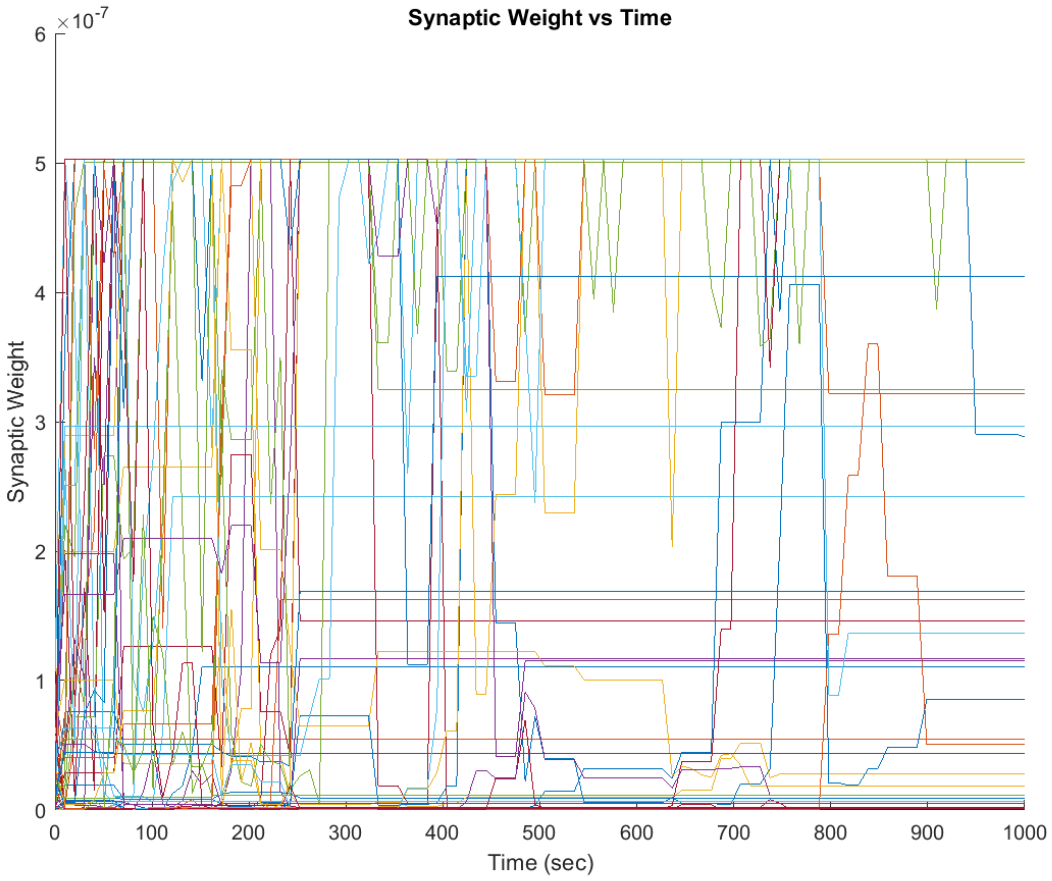

Figure 5.8: A random sample of 50 LTP synapses were graphed with their synaptic weight change over the course of the simulation. The most erratic weight fluctuations occur in the first 250 seconds with some synapses remaining unchanged for the rest of the simulation.

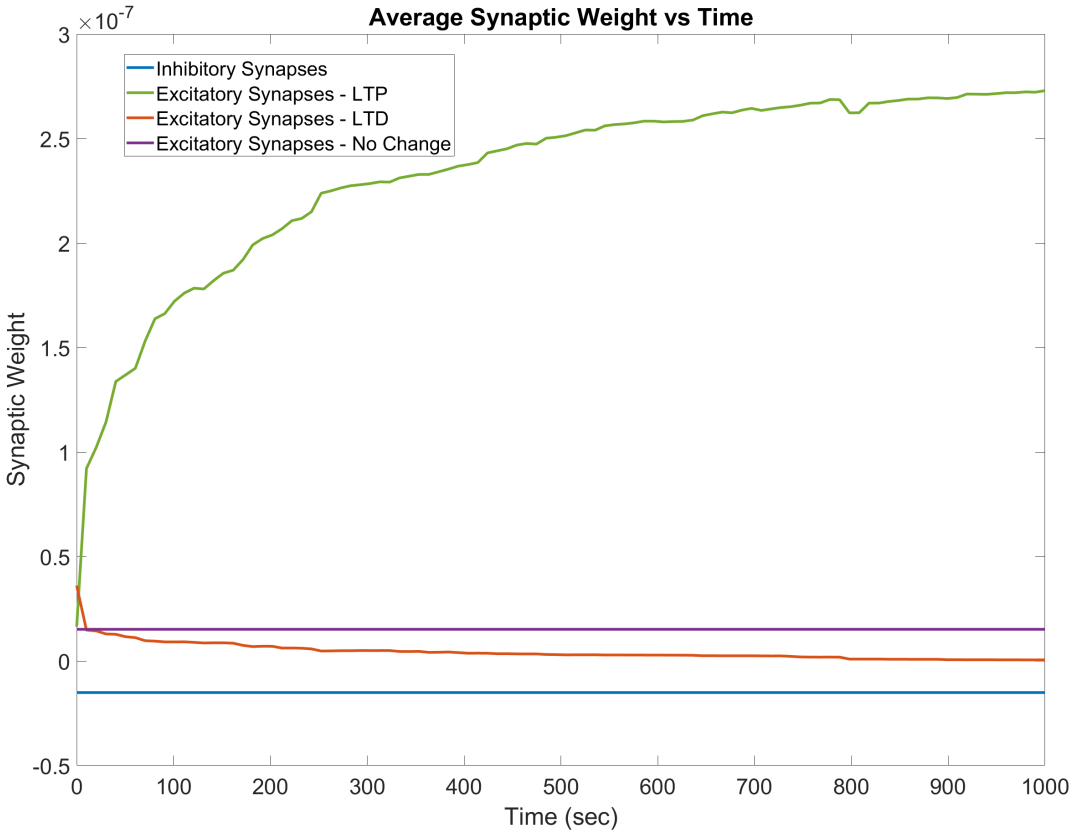

Figure 5.9: Average synaptic weight over time, split by inhibitory and excitatory synapses. Inhibitory synapses experienced no weight change, whereas excitatory synapses experienced both Long Term Depression (LTD) and Long Term Potentiation (LTP).

Table 5.6: Spearman correlation results between weight change trends and presynaptic neuron types.

Weight Change	Presynaptic Neuron Type					
	Endogenously Active		Excitatory		Inhibitory	
	ρ	p-Value	ρ	p-Value	ρ	p-Value
LTP	0.05	< 0.001	0.11	< 0.001	-0.11	< 0.001
LTD	-0.03	< 0.001	0.35	< 0.001	-0.35	< 0.001
No Change	-0.03	< 0.001	-0.65	< 0.001	0.65	< 0.001

5.2.3 Spearman Correlation

Spearman correlation was used to identify any monotonic relationship between synaptic weight change and presynaptic neuron types: endogenously active, excitatory, and inhibitory. There was moderate positive correlation was between synapses weights that did not change and inhibitory presynaptic neurons. This conclusion aligns with the results in Figure 5.9 that show no inhibitory synapses experienced LTD or LTP. There are weak positive correlation results between LTP and LTD for excitatory presynaptic neurons which is likely due to excitatory synapses making up nearly 95% of all synapses. For endogenously active presynaptic neurons, there was negligible correlation found with any long term weight change. All correlations had a near-zero p-value which indicates that the results are not caused by chance.

Chapter 6

DISCUSSION

The comparison of burst summary statistics in Table 5.1 showed that growth bursts are less frequent with four times as many total spikes than bursts during the STDP simulation. The average width for growth bursts is approximately 100 ms wider than STDP bursts. Comparing burst shape in Figure 5.1, contradicts the average width statistic, showing an STDP burst that is approximately three times wider than the growth burst. The dashed line in the right graph shows that APNFR falls below the burst threshold at 0.54 seconds and the final peak is a separate burst that trails burst 14. The temporal proximity of the "trailing" burst indicates that it is likely an aftereffect of the neural activity in burst 14 and its small width causes the lower average width statistic for STDP. This suggests a need to modify the original burst definition from Kawasaki and Stiber to accommodate the new shape of STDP bursts. One proposed modification could require APNFR to remain beneath the burst threshold for a short period of time before terminating a burst. Establishing a reliable burst definition is important for identifying elevated network activity and to further understanding of how information travels through neural pathways.

After the growth simulation, examining synaptic weight showed approximately 95% of synapses were excitatory and only 5% were inhibitory. Synapse type is determined by the presynaptic neuron, so an excitatory presynaptic neuron creates an excitatory synapse with a positive synaptic weight value. As mentioned in Section 3.4.1, the original network was configured with 10% inhibitory neurons, but the network yielded approximately 5% inhibitory connections. This is likely because the connectivity radius of inhibitory neurons grows at half the rate of excitatory neurons, resulting in half as many connections. Given our later results that inhibitory synapses are not changed by STDP, this indicates that networks that

begin with more excitatory neurons are more affected by STDP.

Initial examination of the synaptic weight distribution throughout the STDP simulation revealed no changes until the 13 second mark, subsequent the first burst. The distribution change combined with the burst shape change discovered in Figure 5.2 suggests an interdependence between bursting and the initiation of STDP changes. Consequently, STDP also changes the shape and frequency of network bursts, further demonstrating their mutual effects. This preliminary analysis of how STDP affects bursting behavior helps build an understanding of how important neural pathways are formed. Bursts are a key phenomenon for transmitting information and STDP restructures the network, pruning unnecessary connections, so bursts relay spikes efficiently.

The weight distribution histogram as well as the more granular analysis using boxplots in Figure 5.5, revealed that 79.35% of synaptic weights progressed towards zero. This metric was relatively consistent per-second as shown in Figure 5.6, leading to a hypothesis that LTD synapses will have a consistent decreasing trend in synaptic weight towards zero over time. A synaptic weight of zero indicates that the synapse is unable to transfer information and the synapse is effectively pruned from the network. Although no synapse weights fully reached zero, from Table 5.3, the first quartile value at the end of the simulation is near-zero at 7.29×10^{-44}. Synaptic pruning has been linked to degenerative brain disorders like schizophrenia and Alzheimer's [16, 37]. Identifying pruned synapses can help illuminate the areas most susceptible to these neurological disorders and assist in medical diagnosis.

Since only 9.37% of synapses experience an overall strengthening, this thesis devised a method to isolate these synapses for further investigation by classifying them as LTP synapses. Figure 5.9 shows that the average weight for LTP synapses increases over time, suggesting that LTP synapses form critical neural pathways for transmitting information. Identifying strengthened synapses is the first step towards examining their connections which has applications in designing machine learning architecture to mimic the nervous system. Spiking neural networks (SNNs) currently model neuron spiking behavior for machine learning and applying the learned architecture of LTP synapses could lead to further alignment

between these models and real neural network systems.

Additional examination of synaptic weight changes in Table 5.5 showed a near equal split between excitatory and inhibitory synapses with no weight change. The graph in Figure 5.9 reveals that the average unchanged excitatory synapse weight is 1.51×10^{-8} and the average unchanged inhibitory synapse weight is approximately the additive inverse, -1.51×10^{-8}. Further analysis is required to confirm if these edges encapsulate all the edge pairs between excitatory and inhibitory neurons, where the weighted edges after growth are opposite but equal in magnitude. The unchanged inhibitory synapse weights is consistent with results from experiments *in vivo*, suggesting that inhibitory plasticity is altered through other means [19, 13].

Finally, Spearman correlation was calculated to discern any monotonic relationships between the presynaptic neuron type and long term synaptic weight changes. The strongest correlation was between inhibitory presynaptic neurons and no long term weight change which is consistent with the literature. Additionally, there was weak correlation between excitatory presynaptic neurons and LTD, and a smaller weak correlation between excitatory presynaptic neurons and LTP. These results demonstrate that presynaptic neuron type is a beneficial data point for predicting whether a synapse will be strengthened, weakened, or experience no change as a result of STDP.

Chapter 7

CONCLUSION

This thesis extracted spatiotemporal spiking behavior and weight evolution data from a neural refinement phase simulation implemented with STDP. The exploratory analysis presented in this thesis provides preliminary insight into how STDP affects network behavior when compared to the growth phase. In burst analysis, the addition of STDP to the simulation reshaped bursts from a singular peak of elevated of neuron firing rate to irregular peaks above the burst threshold. Additionally, spatiotemporal visualization revealed that the growth phase burst shape evolved from a circular propagation expanding from an origin point to multiple wave fronts firing throughout the network.

In synaptic weight analysis, approximately 71% of synapse weights decreased towards zero over time. The synapses that increased in weight saw irregular weight fluctuations with select synapse weights stabilizing over time. Lastly, Spearman correlation was calculated between the presynaptic neuron type and whether a synapse experienced LTD or LTP. There was a statistically significant positive correlation between inhibitory presynaptic neurons and no weight change as well as a smaller positive correlation between excitatory presynaptic neurons and weights that experienced LTP or LTD. There was no significant correlation between weight change and endogenously active presynaptic neurons.

The analysis presented in this thesis provides a foundational framework for understanding how STDP affects neural network behavior. The method presented to distinguish long term synapse effects demonstrated how to identify pruned synapses versus strengthened synapses. Further research into the pruned synapses could lead to insights about neurodegenerative diseases and examination of strengthened synapses has applications in designing machine learning architecture.

Chapter 8

FUTURE WORK

First, the breadth of this research can be expanded by applying the data analysis pipeline to other simulation configurations known to exhibit bursting behavior to see if the effects of STDP are consistent across simulations. Growth simulations with bursting behavior include neuron graphs with 98% excitatory cells or a target rate of 1.9Hz [18].

This work offered initial insights into the correlation between presynaptic neuron types and synaptic weight. Further research can continue to investigate the intersection of network structure and synaptic weight change by combining burst and weight analysis with the graph analysis presented in Singh 2021 [32]. Applying graph analysis specifically to the LTP synapses would be beneficial towards designing machine learning architecture that aligns with systems developed in living organisms. Since SNNs mimic the spiking behavior seen in neural networks, they could further model neural development by applying LTP synapse architecture for improved performance.

Currently, the STDP implementation is only available on CPU and not GPU, resulting in memory and time constraints in running the simulation. Implementing STDP on GPU would allow for granular analysis of the relationship between network bursts and weight change. Further investigation is required to define the interdependent relationship between bursts and STDP and ensure that the results align with network-timing-dependent plasticity research [8].

Finally, the abundance of data output by Graphitti is a prime candidate for machine learning research and this thesis presented a data analysis pipeline consistent with data preparation for machine learning. Potential classification problems include using ML to predict which synapses will be pruned from the network, a process that has been linked

to several illnesses including schizophrenia and Alzheimer's disease [16, 37]. For multi-class classification, ML could be used for predicting if a synapse will experience LTP, LTD, or no weight change. Similar to the Spearman correlation analysis, machine learning is also helpful for analyzing which input variables contribute more information to predicting a result. Identifying the relationship between neural network structure and long term synapse effects may provide insight for early medical diagnoses of neural structures that are more susceptible to degeneration.

BIBLIOGRAPHY

[1] Bruce Alberts, Alexander Johnson, Julian Lewis, Martin Raff, Keith Roberts, and Peter Walter. Neural Development. In *Molecular Biology of the Cell. 4th edition*. Garland Science, 2002.

[2] Derek William Schneider Arthur. Effect of Spike-Timing Dependent Plasticity Rule Choice on Memory Capacity and Form in Spiking Neural Networks. Master's thesis, University of Lethbridge (Canada), Canada – Alberta, CA, 2023. ISBN: 9798381685213.

[3] William Bechtel. The Endogenously Active Brain: The Need for an Alternative Cognitive Architecture. *Philosophia Scientiæ. Travaux d'histoire et de philosophie des sciences*, (17-2):3–30, May 2013. ISBN: 9782841746316 Number: 17-2 Publisher: Université Nancy 2.

[4] Curtis C. Bell, Victor Z. Han, Yoshiko Sugawara, and Kirsty Grant. Synaptic plasticity in a cerebellum-like structure depends on temporal order. *Nature*, 387(6630):278–281, May 1997. Publisher: Nature Publishing Group.

[5] Guo-qiang Bi and Mu-ming Poo. Synaptic Modifications in Cultured Hippocampal Neurons: Dependence on Spike Timing, Synaptic Strength, and Postsynaptic Cell Type. *Journal of Neuroscience*, 18(24):10464–10472, December 1998. Publisher: Society for Neuroscience Section: ARTICLE.

[6] Guoqiang Bi and Mu-ming Poo. Synaptic modification by correlated activity: Hebb's postulate revisited. *Annual review of neuroscience*, 24:139–66, 02 2001.

[7] Michela Chiappalone, Alessandro Vato, Luca Berdondini, Milena Koudelka-Hep, and Sergio Martinoia. Network dynamics and synchronous activity in cultured cortical neurons. *International Journal of Neural Systems*, 17(02):87–103, April 2007. Publisher: World Scientific Publishing Co.

[8] Vincent Delattre, Daniel Keller, Matthew Perich, Henry Markram, and Eilif Benjamin Muller. Network-timing-dependent plasticity. *Frontiers in Cellular Neuroscience*, 9, June 2015. Publisher: Frontiers.

[9] Ryan N. Delgado, Denise E. Allen, Matthew G. Keefe, Walter R. Mancia Leon, Ryan S. Ziffra, Elizabeth E. Crouch, Arturo Alvarez-Buylla, and Tomasz J. Nowakowski. Individual human cortical progenitors can produce excitatory and inhibitory neurons. *Nature*, 601(7893):397–403, January 2022. Publisher: Nature Publishing Group.

[10] Jean-Pierre Eckmann, Ofer Feinerman, Leor Gruendlinger, Elisha Moses, Jordi Soriano, and Tsvi Tlusty. The physics of living neural networks. *Physics Reports*, 449(1):54–76, September 2007.

[11] Christopher D. Fiorillo, Jaekyung K. Kim, and Su Z. Hong. The meaning of spikes from the neuron's point of view: predictive homeostasis generates the appearance of randomness. *Frontiers in Computational Neuroscience*, 8:49, April 2014.

[12] Robert C. Froemke and Yang Dan. Spike-timing-dependent synaptic modification induced by natural spike trains. *Nature*, 416(6879):433–438, March 2002.

[13] Robert C. Froemke, Michael M. Merzenich, and Christoph E. Schreiner. A synaptic memory trace for cortical receptive field plasticity. *Nature*, 450(7168):425–429, November 2007. Publisher: Nature Publishing Group.

[14] Önder Gürcan, Oğuz Dikenelli, and Kemal S. Türker. Agent-based Exploration of Wirings of Biological Neural Networks: Position Paper, September 2012. arXiv:1209.3150 [cs].

[15] D. O. Hebb. *The Organization of Behavior: A Neuropsychological Theory*. Psychology Press, Oxford, 1 edition, 2005.

[16] Oliver D. Howes and Ellis Chika Onwordi. The synaptic hypothesis of schizophrenia version III: a master mechanism. *Molecular Psychiatry*, 28(5):1843–1856, May 2023. Publisher: Nature Publishing Group.

[17] Eric R. Kandel. Nerve Cells, Neural Circuitry, and Behavior. In *Principles of neural science*, pages 21–38. McGraw-Hill, New York, 5th ed edition, 2013.

[18] Fumitaka Kawasaki and Michael Stiber. A simple model of cortical culture growth: burst property dependence on network composition and activity. *Biological Cybernetics*, 108(4):423–443, August 2014.

[19] Rylan S. Larsen, Deepti Rao, Paul B. Manis, and Benjamin D. Philpot. STDP in the Developing Sensory Neocortex. *Frontiers in Synaptic Neuroscience*, 2:9, June 2010.

[20] Jewel (Yun-Hsuan) Lee. Machine Learning of Spatiotemporal Bursting Behavior in Developing Neural Networks. Master's thesis, University of Washington, 2018.

[21] W. B. Levy and O. Steward. Temporal contiguity requirements for long-term associative potentiation/depression in the hippocampus. *Neuroscience*, 8(4):791–797, 1983. Place: United States Publisher: Elsevier Ltd.

[22] J. E. Lisman. Bursts as a unit of neural information: making unreliable synapses reliable. *Trends in Neurosciences*, 20(1):38–43, January 1997.

[23] Larry J. Millet and Martha U. Gillette. Over a Century of Neuron Culture: From the Hanging Drop to Microfluidic Devices. *The Yale Journal of Biology and Medicine*, 85(4):501–521, December 2012.

[24] António R. C. Paiva, Il Park, and José C. Príncipe. Chapter 8 - Inner Products for Representation and Learning in the Spike Train Domain. In Karim G. Oweiss, editor, *Statistical Signal Processing for Neuroscience and Neurotechnology*, pages 265–309. Academic Press, Oxford, January 2010.

[25] Jerome Pine. Recording action potentials from cultured neurons with extracellular microcircuit electrodes. *Journal of Neuroscience Methods*, 2(1):19–31, February 1980.

[26] Jessy Presumey, Allison R. Bialas, and Michael C. Carroll. Chapter Two - Complement System in Neural Synapse Elimination in Development and Disease. In Frederick W. Alt, editor, *Advances in Immunology*, volume 135, pages 53–79. Academic Press, January 2017.

[27] Dale Purves, George J. Augustine, David Fitzpatrick, Lawrence C. Katz, Anthony-Samuel LaMantia, James O. McNamara, and S. Mark Williams. Excitatory and Inhibitory Postsynaptic Potentials. In *Neuroscience. 2nd edition*. Sinauer Associates, 2001.

[28] Dale Purves, George J. Augustine, David Fitzpatrick, Lawrence C. Katz, Anthony-Samuel LaMantia, James O. McNamara, and S. Mark Williams. The Refractory Period. In *Neuroscience. 2nd edition*. Sinauer Associates, 2001.

[29] Sanaullah, Shamini Koravuna, Ulrich Rückert, and Thorsten Jungeblut. Exploring spiking neural networks: a comprehensive analysis of mathematical models and applications. *Frontiers in Computational Neuroscience*, 17, August 2023. Publisher: Frontiers.

[30] Harel Z. Shouval, Samuel S. Wang, and Gayle M. Wittenberg. Spike Timing Dependent Plasticity: A Consequence of More Fundamental Learning Rules. *Frontiers in Computational Neuroscience*, 4, July 2010. Publisher: Frontiers.

[31] Smriti Singh. Understanding localized burst trigger patterns in developing neural networks using deep learning. Master's thesis, University of Washington, 2020.

[32] Snigdha Singh. Graph Analysis For Simulated Neural Networks With STDP. Master's thesis, University of Washington, 2021.

[33] Sen Song, Kenneth D. Miller, and L. F. Abbott. Competitive Hebbian learning through spike-timing-dependent synaptic plasticity. *Nature Neuroscience*, 3(9):919–926, September 2000. Publisher: Nature Publishing Group.

[34] Jyothsna Suresh, Mihailo Radojicic, Lorenzo L. Pesce, Anita Bhansali, Janice Wang, Andrew K. Tryba, Jeremy D. Marks, and Wim van Drongelen. Network burst activity in hippocampal neuronal cultures: the role of synaptic and intrinsic currents. *Journal of Neurophysiology*, 115(6):3073–3089, June 2016.

[35] Christopher Brian Thornton. *Simulation and Analysis of Stimulus Evoked and Seizure-like Activity in an Acute Rat Neocortical Brain Slice Preparation.* Thesis, Newcastle University, 2020. Accepted: 2021-09-10T14:01:02Z.

[36] Daniel A. Wagenaar, Jerome Pine, and Steve M. Potter. An extremely rich repertoire of bursting patterns during the development of cortical cultures. *BMC Neuroscience*, 7(1):11, February 2006.

[37] Lang Wen, Danlei Bi, and Yong Shen. Complement-mediated synapse loss in Alzheimer's disease: mechanisms and involvement of risk factors. *Trends in Neurosciences*, 47(2):135–149, February 2024.

[38] Kashu Yamazaki, Viet-Khoa Vo-Ho, Darshan Bulsara, and Ngan Le. Spiking Neural Networks and Their Applications: A Review. *Brain Sciences*, 12(7):863, June 2022.